LA-UR-21-22325
Approved for public release; distribution is unlimited.

Title: (U) Segmented Scintillator Pitch, Thickness, and Septa Material Effects on the Swank Factor, Quantum Efficiency, and DQE(0) for High-Energy X-Ray Radiography

Author(s): Disterhaupt, Jennifer Lynn Schei
James, Michael R.
Klasky, Marc Louis

Intended for: Report

Issued: 2021-03-09

(U) Segmented Scintillator Pitch, Thickness, and Septa Material Effects on the Swank Factor, Quantum Efficiency, and DQE(0) for High-Energy X-Ray Radiography

Jennifer L. Schei, Michael R. James, and Marc L. Klasky
Los Alamos National Laboratory
Los Alamos, NM 87545
February 2021

LA-UR-21-XXXXX

Contents

Contents **2**

List of Figures **3**

List of Tables **4**

1 Executive Summary **5**

2 Background **6**

3 Methods **6**
3.1 Spectrum 6
3.2 Scintillator Model 8
3.3 Calculating the Detector Response 11

4 Results **12**
4.1 Spectra 12
4.2 Detector Responses for Cobalt 60 Source 14
4.3 Detector Responses for 20 MeV Spectrum Filtered by a Flat Field 18
4.4 Detector Responses for 22.4 MeV Spectrum Filtered by a Flat Field 21
4.5 Detector Responses for 20 MeV Spectrum Filtered by an FTO 23
4.6 Detector Responses for 22.4 MeV Spectrum Filtered by an FTO 26

5 Conclusions **29**

References **32**

List of Figures

1 Spectrum Setup 1 7
2 Spectrum Setup 2 8
3 Scintillator Design 9
4 Scintillator Layout 10
5 Swank Calculation Example 12
6 Endpoint Energy: Flat Field Spectra 13
7 Endpoint Energy: Flat Field Total Spectra 13
8 Endpoint Energy: FTO Spectra 14
9 Endpoint Energy: FTO Total Spectra 14
10 Co60: Detector Response 15
11 Co60: Detector Response Pixel Pitch Differences 16
12 Co60: Detector Response Septa Material Differences 16
13 Co60: Detector Response Scintillator Material Differences 17
14 Co60: Detector Response Scintillator Thickness Differences 17
15 20MeV Flat Field: Detector Response 19
16 20MeV Flat Field: Detector Response Pixel Pitch Differences 19
17 20MeV Flat Field: Detector Response Septa Material Differences 20
18 20MeV Flat Field: Detector Response Scintillator Thickness Differences . . . 20
19 22.4 MeV Flat Field: Detector Response 22
20 22.4 MeV Flat Field: Detector Response Pixel Pitch Differences 22
21 22.4 MeV Flat Field: Detector Response Septa Material Differences 23
22 22.4 MeV Flat Field: Detector Response Scintillator Thickness Differences . 23
23 20 MeV FTO: Detector Response 25
24 20 MeV FTO: Detector Response Pixel Pitch Differences 25
25 20 MeV FTO: Detector Response Septa Material Differences 26
26 20 MeV FTO: Detector Response Scintillator Thickness Differences 26
27 22.4 MeV FTO: Detector Response 28
28 22.4 MeV FTO: Detector Response Pixel Pitch Differences 28
29 22.4 MeV FTO: Detector Response Septa Material Differences 29
30 22.4 MeV FTO: Detector Response Scintillator Thickness Differences 29

List of Tables

1 Scintillator Materials 9
2 Scintillator Geometries 10
3 Material Composition 10
4 Material Composition 11
5 Scintillator Irradiation Area 11
6 Endpoint Energy: Flat Field Scatter-to-Direct Ratio 12
7 Endpoint Energy: FTO Scatter-to-Direct Ratio 13
8 Source: Co60 1.095 mm pixel pitch 15
9 Source: Co60 1.302 mm pixel pitch 15
10 Source: 20 MeV Flat Field 1.095 mm pixel pitch 18
11 Source: 20 MeV Flat Field 1.302 mm pixel pitch 18
12 Source: 22.4 MeV Flat Field 1.095 mm pixel pitch 21
13 Source: 22.4 MeV Flat Field 1.302 mm pixel pitch 21
14 Source: 20 MeV FTO 1.095 mm pixel pitch 24
15 Source: 20 MeV FTO 1.302 mm pixel pitch 24
16 Source: 22.4 MeV FTO 1.095 mm pixel pitch 27
17 Source: 22.4 MeV FTO 1.302 mm pixel pitch 27
18 Scintillator Geometry Rankings 31

1 Executive Summary

Scintillator design is an important aspect in constructing a radiographic facility in order to collect the most robust data possible. For the proposed Enhanced Capabilities for Subcritical Experiment (ECSE) facility in Nevada, we explored a permutation of 13 segmented scintillator designs in order to understand the best performance and trade offs for each design. We calculated the quantum efficiency, Swank factor, and detective quantum efficiency at zero-frequency (DQE(0)) for each scintillator design in order to compare performance.

The scintillator designs we investigated varied the pixel pitch, 1.095 mm and 1.302 mm; the septa material, stainless steel and tungsten alloy; and the scintillator thickness, 40 mm, 45 mm, and 50 mm. In addition, we compared the detector response using lutetium oxyorthosilicate (LSO) and lutetium-yttrium oxyorthosilicate (LYSO) for one design. We compared the detector responses using five different sources: cobalt 60, 20 MeV filtered by a flat field with 7 cm tungsten in the bullnose, 22.4 MeV filtered by a flat field with 7 cm tungsten in the bullnose, 20 MeV filtered by an FTO with four plates, and 22.4 MeV filtered by an FTO with four plates.

We calculated the poly-energetic spectra using the dual-axis radiographic hydrodynamic test facility (DARHT) line-of-sight (LOS) materials present following the instillation of the weather enclosure in 2020. The direct, scattered, and total radiation were calculated and the total radiation was used to calculate the detector responses. The scatter-to-direct ratios for the spectra filtered by a flat field were $\approx$0.3–0.4, while the scatter-to-direct ratios for the spectra filtered by an FTO were much larger, $\approx$1.1–1.3. This larger ratio may be due to the object producing more scatter and the removal of the gamma-ray camera (GRC) blast shield that may have served to attenuate some scatter [4].

The detector responses using a cobalt 60 source will serve to validate these calculations with experimental measurements. We compared our results with those calculated by the University of Michigan using EGSnrc and EGS++ and found very good agreement. Some simplifications in the calculations such as using a single x-ray energy of 1.25 instead of the dual-energy of 1.17 and 1.33, as well as illuminating the central region of the scintillator to give a theoretical detector response, will yield differences between these calculations and the experimental measurements. In general, we found that DQE(0) was largest for the larger pixel pitch (1.302 mm), stainless steel septa, and the thickest scintillator design.

Using the poly-energetic data, we found that DQE(0) was largest for the larger pixel pitch (1.302 mm), tungsten alloy septa, and the thickest scintillator design. The impact of the different scintillator designs on the Swank factor was small ($\approx$1–2%) whereas the impact on the quantum efficiency was much larger ($\approx$4–10%). The largest trade off for increasing DQE(0) resulted from using tungsten alloy septa material ($\approx$4–10%) and increasing the scintillator thickness ($\approx$5–12%). Modifying the pixel pitch had a smaller effect on DQE(0) ($\approx$1–2%).

For a cobalt 60 source, the largest DQE(0) resulted from a 1.302 mm pixel pitch, stainless steel septa, and 50 mm thick scintillator. However, the poly-energetic sources had the largest DQE(0) for a 1.302 mm pixel pitch, tungsten alloy septa, and 50 mm thick scintillator. Since the scintillator design is intended for a high-energy x-ray source, it is recommended to use the optimized results from the poly-energy calculations. The cobalt 60 data serve to validate the calculations with experimental data as it is more feasible to acquire than the poly-energetic

data.

A ranking of the scintillator designs that produce the largest DQE(0) for the poly-energetic sources are listed in Table 18. In the event of manufacturing limitations, this table lists the preferential order of scintillator design based upon DQE(0) calculations. It is important to consider the frequency-dependent DQE along with the contributions from optical photons in the final scintillator design choice.

2 Background

X-ray radiography is used to capture images of imploding materials across time, in order to aid in our understand of dynamic material behavior. In these regimes, high-energy x-rays are required to penetrate the dense materials and form a radiographic image. As part of the system design, we are investigating the effects of different segmented scintillator geometries and materials on the detector response. Comparing these calculations provides relative comparisons between scintillator designs.

The purpose of this study is to compare different scintillator designs for use at the proposed ECSE facility in Nevada. Optimizing the scintillator design will allow for the collection of the most robust data possible.

To quantify the detector response, we calculated the quantum efficiency, Swank factor, and DQE(0). The quantum efficiency is the sum of the zeroth moment across energies. The Swank factor accounts for the different absorbed photon energies for an incident energy spectrum. The DQE(0) is the product of the quantum efficiency and the Swank factor. Five different source spectra were used to calculate the detector responses. We calculated the detector response using a cobalt 60 source so that we can easily produce experimental data to validate the calculations. We used four different poly-energy spectra to calculate the detector response. A 20 MeV spectra filtered by a flat field, employed at DARHT, may potentially be used in for calculation validation as well. A 20 MeV spectra filtered by an FTO with four plates gives the detector response for a spectra in a regime of interest. A 22.4 MeV spectra will be employed at ECSE and thus gives detector responses for the facility in which the scintillator is being designed.

3 Methods

The spectra generation and detector responses were calculated using MCNP6 [2]. Below we describe our methods in detail.

3.1 Spectrum

To calculate the detector response for different geometries and materials, we used five different sources. The first source was a cobalt 60 source. These calculations used a mono-energetic source of 1.25 MeV in order to compare with calculations from the University of Michigan using EGSnrc and EGS++. While the detector response is quite different at relatively low energies, these calculations will be used for validation against experimental data. A cobalt

60 source has dual energies at 1.17 and 1.33 MeV, and our simplification of a single energy may introduce uncertainty between the calculation and experimental data.

We also used four poly-energetic spectra to calculate the detector responses. These include:

- 20 MeV bremsstrahlung spectrum filtered by a flat field with 7 cm tungsten in the bullnose,
- 22.4 MeV bremsstrahlung spectrum filtered by a flat field with 7 cm tungsten in the bullnose,
- 20 MeV bremsstrahlung spectrum filtered by an FTO with four plates, and
- 22.4 MeV bremsstrahlung spectrum filtered by an FTO with four plates.

We calculated the poly-energetic spectra using the DARHT LOS materials for those present after the installment of the weather enclosure in 2020. This includes the removal of the gamma-ray camera (GRC) blast shield and the near-detector materials. We did not include surrounding material far from the LOS, such as the floor and walls as these materials would make it difficult to achieve convergence of our calculations in a reasonable computational time frame. Figure 1 shows the upstream portion of the DARHT configuration where the source enters from the left side of the diagram. Figure 2 shows the downstream portion of the DARHT configuration. The spectrum was captured on the far-right portion of the setup.

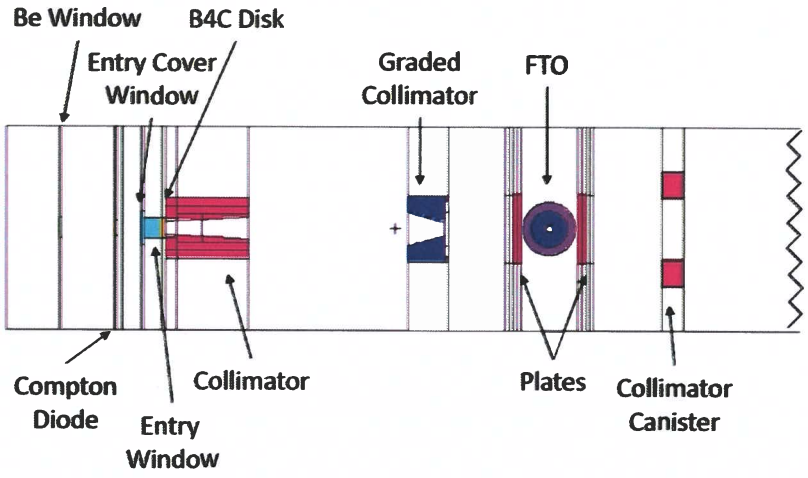

Figure 1: The upstream half of the DARHT line-of-sight materials and configuration used to calculate the energy spectrum.

We generated initial bremsstrahlung spectra with end-point energies of 20 MeV and 22.4 MeV by impinging electrons onto a tungsten converter target and recording the photon energy spectrum. Then, using the resulting two spectra, we generated output spectra that were filtered by the DARHT LOS configurations for a flat field and a French Test Object

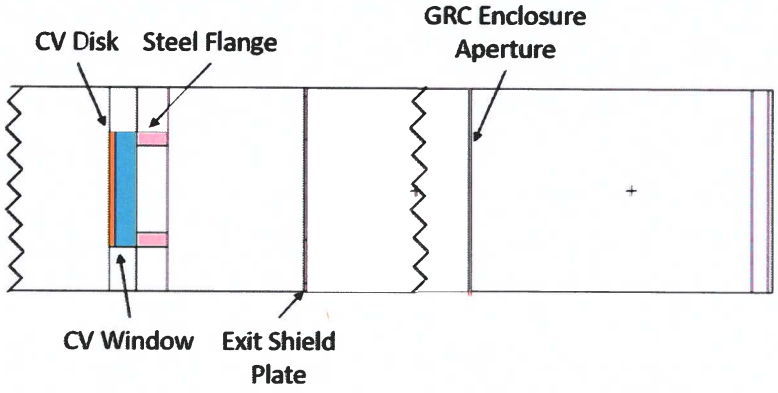

Figure 2: The downstream half of the DARHT line-of-sight materials and configuration used to calculate the energy spectrum.

(FTO) with four plates. For the flat field filtration, the FTO and plates were removed, and 7 cm of tungsten material was placed in the bullnose. We generated four different energy spectra that were used to characterize the detector responses.

The 20 MeV spectrum filtered by a flat field is the current spectrum at DARHT Axis 1 and this may be used to validate the calculations with experimental data. The 22.4 MeV spectrum filtered by a flat field would be the spectrum produced at ECES and will be used to calculate scintillator performance for that facility. The 20 MeV and 22.4 MeV spectra filtered by an FTO with four plates gives an indication of the scintillator performance in a closer approximation of the desired regime. While these calculations cannot be validated with experiments, they can be used for relative comparison in scintillator design.

The direct, scattered, and total radiation were calculated for each poly-energetic configuration. To calculate the detector response, the total radiation spectra were used in all cases in order to model for the most realistic spectra that would be observed experimentally.

We made some modeling simplifications for the incoming beam. The incident beam was parallel and the spot size, resulting in source blur, was not modeled. The spectrum energy and fluence was not varied across the image, as would typically be the case for an object such as the FTO. Rather, we utilized a single spectrum across the entire scintillator to assess the performance. We have previously shown that the angular dependence of the scattered radiation has a negligible effect on the detector response [4] and therefore was not included in this study.

3.2 Scintillator Model

The scintillator model was comprised of seven materials in direct contact with each other [1] and are listed in Table 1. For each calculation, either LSO or LYSO was used as the scintillating material and either stainless steel or tungsten alloy was used as the septa material. The scintillator thickness was varied between 40 mm, 45 mm, and 50 mm to understand the effects on performance. This scintillator design package will be employed at DARHT following the instillation of the weather enclosure in 2020. A schematic of this detector package is

illustrated in Figure 3.

Table 1: The scintillator material layers that comprised the detector model.

Material	Thickness (mm)	Density (g/cc)
Carbon Fiber Clamp	0.5461	1.61
Polyurethane Foam Pad	0.3175	1.005
Tantalum	0.0508	16.53
Teflon	0.0254	2.2
LSO Scintillator	40, 45, or 50	7.4
LYSO Scintillator	40, 45, or 50	7.1
Stainless Steel Septa	40, 45, or 50	8.03
Tungsten Alloy Septa	40, 45, or 50	19.3
Acetate Film	0.0254	1.0446
BK7 Glass	1.27	2.51

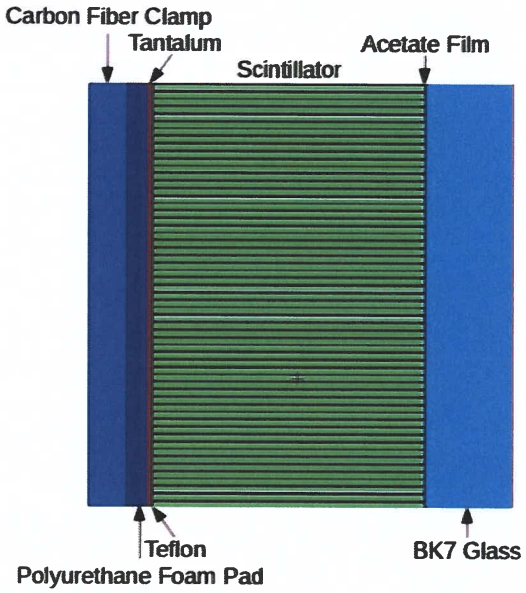

Figure 3: The scintillator was modeled with four materials upstream of the scintillator and two materials downstream of the scintillator, all in contact.

We also varied the geometry of the segmented scintillator where the pitch was either 1.095 mm or 1.302 mm (Table 2). The larger pitch results in a larger scintillating area. A schematic of the scintillator geometry is shown in Figure 4.

Building the MCNP models, we used the chemical formulas listed in Table 3 and compositions listed in Table 4.

We irradiated the center region of the scintillator with a linear falloff to allow for scatter within the scintillator to not be lost due to edge effects, which gives a theoretical value of the

Table 2: The two different scintillator geometry specifications.

	First Geometry	Second Geometry
Pitch	1.095 mm	1.302 mm
Scintillator Size	0.845 mm	1.052 mm
Total Air Gap	60 μm	60 μm
Septa Wall Thickness	190 μm	190 μm

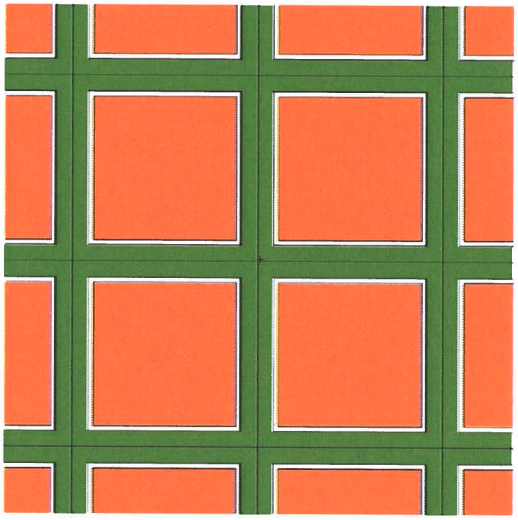

Figure 4: The model of the segmented scintillator where green is the septa material, white is the air gap, and orange is the scintillator crystal.

Table 3: The materials and chemical formulas.

Material	Chemical Formula
Polyurethane	$C_3H_8N_2O$-
Tantalum	Ta
Teflon	F_4C_2-
LSO	Lu_2SiO_5
LYSO	$Lu_{1.8}Y_{0.2}SiO_5$:Ce
Acetate	$C_2H_3O_2$-

quantum efficiency Swank factor, and DQE(0). The details of the scintillator area, irradiation area, and region of interest (ROI) are listed in Table 5. This was chosen in order to compare our calculations using MCNP6 to those performed by the University of Michigan using EGSnrc and EGS++. These detector response calculations will provide a theoretical value; however, we expect that they will slightly differ in comparison to experimental measurements since the entire scintillator will be irradiated in the experimental setup.

We made some general simplifications regarding the detector model. The scintillator had a regular geometry, not a half pixel offset as is the case with the scintillator utilized at DARHT until 2019. Additionally, the scintillator elements were not focused.

Table 4: The material composition of element percentage.

Carbon Fiber		BK7 Glass		Tungsten Alloy MT-185		Stainless Steel	
Element	%	Element	%	Element	%	Element	%
C	85.7	Si	32.315	W	99.95	Fe	71.492
H	2.6	B	3.339	C	0.00834	C	0.021
Cl	3.6	Ba	2.75	O	0.00834	Mn	1.31
O	8.1	Na	7.715	N	0.00833	Si	0.42
		K	5.222	Fe	0.00833	P	0.024
		As	0.273	Ni	0.00833	S	0.001
		O	48.387	Si	0.00833	Cr	18.16
						Ni	8.0
						Mo	0.22
						N	0.072
						Cu	0.28

Table 5: The scintillator area, irradiation area, and region of interest (ROI) used to calculate the detector responses.

Pixel Pitch	Scintillator Area	Irradiation Area	ROI
1.095 mm	24 × 24 cm^2	6 cm radius	24 × 24 cm^2
1.302 mm	24 × 24 cm^2	6 cm radius	24 × 24 cm^2

3.3 Calculating the Detector Response

We have previously tested our MCNP models against the original Swank paper to verify our models with published results and have described our methods in detail [4]. We briefly give an overview of our methods here. For each energy bin, we used an F8 Tally (pulse-height spectrum) to calculate the moments of the scintillator pulse height distribution. The quantum efficiency is defined as,

$$A_Q = M_0, \tag{1}$$

where M_0 is the zeroth moment of the scintillator pulse-height distribution. The Swank factor is defined as,

$$I(E) = \frac{M_1^2(E)}{M_0(E)M_2(E)}, \tag{2}$$

where M_0, M_1, and M_2 are the moments of the scintillator pulse-height distribution [3]. Swank specifically notes that in order to accurately calculate the Swank factor for an energy distribution, the moments must be calculated for each incident energy and weight the moments by the input spectrum in order to calculate I. For each energy bin, we calculated the normalized flux for the incident energy spectrum. Then, we calculated the weighted moments, based on the normalized flux for each energy bin, and summed across the energy spectrum. The Swank factor was then calculated from the sum of the weighted moments. An example of the weighted moments calculations in a spreadsheet is shown in Figure 5.

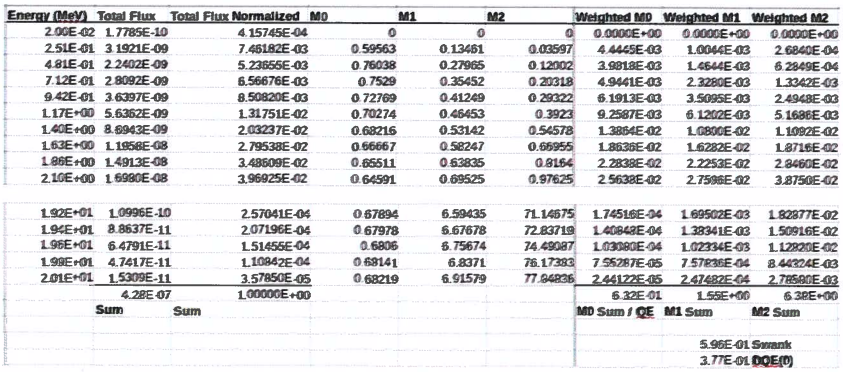

Energy (MeV)	Total Flux	Total Flux Normalized	M0	M1	M2	Weighted M0	Weighted M1	Weighted M2
2.00E-02	1.7785E-10	4.15745E-04	0	0	0	0.0000E+00	0.0000E+00	0.0000E+00
2.51E-01	3.1921E-09	7.46182E-03	0.59563	0.13461	0.03597	4.4445E-03	1.0044E-03	2.6840E-04
4.81E-01	2.2402E-09	5.23655E-03	0.76038	0.27965	0.12002	3.9818E-03	1.4644E-03	6.2849E-04
7.12E-01	2.8092E-09	6.56676E-03	0.7529	0.35452	0.20318	4.9441E-03	2.3280E-03	1.3342E-03
9.42E-01	3.6397E-09	8.50820E-03	0.72769	0.41249	0.29322	6.1913E-03	3.5095E-03	2.4948E-03
1.17E+00	5.6362E-09	1.31751E-02	0.70274	0.46453	0.3923	9.2587E-03	6.1202E-03	5.1686E-03
1.40E+00	8.6943E-09	2.03237E-02	0.68216	0.53142	0.54578	1.3864E-02	1.0806E-02	1.1092E-02
1.63E+00	1.1958E-08	2.79538E-02	0.66667	0.58247	0.66955	1.8638E-02	1.6282E-02	1.8716E-02
1.86E+00	1.4913E-08	3.48609E-02	0.65511	0.63835	0.8164	2.2838E-02	2.2253E-02	2.8460E-02
2.10E+00	1.6980E-08	3.96925E-02	0.64591	0.69525	0.97625	2.5638E-02	2.7596E-02	3.8750E-02
1.92E+01	1.0996E-10	2.57041E-04	0.67894	6.59435	71.14675	1.74516E-04	1.69502E-03	1.82877E-02
1.94E+01	8.8637E-11	2.07196E-04	0.67978	6.67678	72.83719	1.40848E-04	1.38341E-03	1.50916E-02
1.98E+01	6.4791E-11	1.51455E-04	0.6806	6.75674	74.49087	1.03080E-04	1.02334E-03	1.12826E-02
1.99E+01	4.7417E-11	1.10842E-04	0.68141	6.8371	76.17393	7.55287E-05	7.57836E-04	8.44324E-03
2.01E+01	1.5309E-11	3.57850E-05	0.68219	6.91579	77.84836	2.44122E-05	2.47482E-04	2.78580E-03
	4.28E-07	1.00000E+00				6.32E-01	1.55E+00	6.38E+00
	Sum	Sum				M0 Sum / QE	M1 Sum	M2 Sum
							5.96E-01	Swank
							3.77E-01	DQE(0)

Figure 5: A spreadsheet showing the calculation of the moments for each energy bin as well as the calculation of the quantum efficiency, Swank factor, and DQE(0).

DQE(0) is defined as the product of the quantum efficiency and the Swank factor,

$$DQE(0) = M_0 \cdot \frac{M_1^2(E)}{M_0(E)M_2(E)}. \tag{3}$$

4 Results

The poly-energetic spectra generated for 20 MeV and 22.4 MeV endpoint energies as well as the detector responses for each of the five source spectra are shown below.

4.1 Spectra

We calculated four poly-energetic spectra that included two different endpoint energies and two different filtration setups. These spectra were used to calculate and compare the detector responses for different scintillator geometries and material compositions. The direct, scattered, and total radiation are shown for each of the four spectra.

Figure 6 shows the spectra filtered by a flat field for 20 MeV and 22.4 MeV endpoint energy spectra. A comparison of the total spectra for the two different endpoint energies is shown in Figure 7. These two spectra are nearly identical from 0–17 MeV and then begin to diverge at the different endpoint energies. The scatter-to-direct ratios are around 0.3–0.4 for beams filtered by a flat field.

Table 6: The scatter-to-direct ratios for the two different endpoint energy spectra filtered by a flat field with 7cm of tungsten in the bullnose.

Endpoint Energy	Scatter-to-Direct Ratio
20 MeV	0.30
22.4 MeV	0.37

The 20 MeV and 22.4 MeV spectra filtered by an FTO are shown in Figure 8 and a comparison of the total spectra are shown in Figure 9. The two spectra are nearly identical

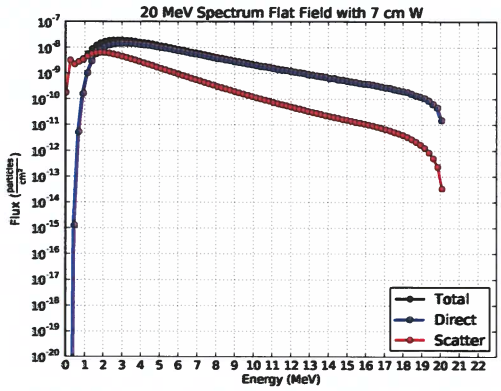

(a) 20 MeV Flat Field Spectrum

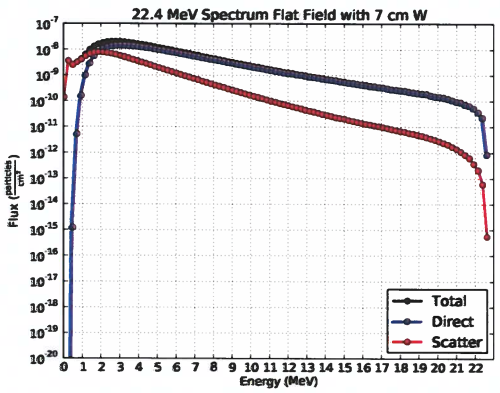

(b) 22.4 MeV Flat Field Spectrum

Figure 6: Direct, scatter, and total radiation spectra filtered by a flat field with 7 cm of tungsten in the bullnose for two different endpoint energies.

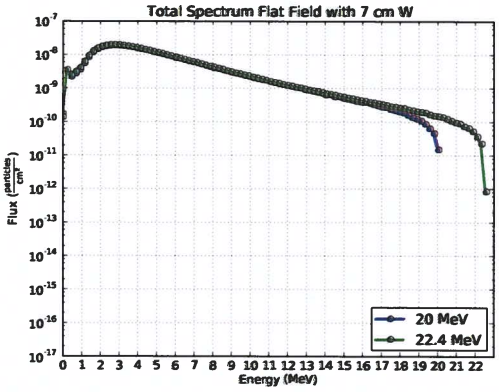

Figure 7: Total radiation spectra filtered by a flat field with 7 cm of tungsten in the bullnose for two different endpoint energies.

from 0–17 MeV and then diverge until the endpoint energies. The scatter-to-direct ratios are much larger for the spectra filtered by the FTO, around 1.1–1.3, compared to the spectra filtered by the flat field. This may be due to the removal of the GRC blast shield, which may have acted to attenuate scattered radiation from the object and reduce the amount that reached the detector.

Table 7: The scatter-to-direct ratios for the two different endpoint energy spectra filtered by an FTO with 4 plates.

Endpoint Energy	Scatter-to-Direct Ratio
20 MeV	1.09
22.4 MeV	1.27

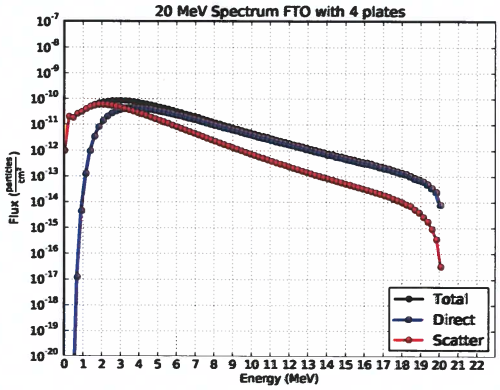

(a) 20 MeV FTO Spectrum

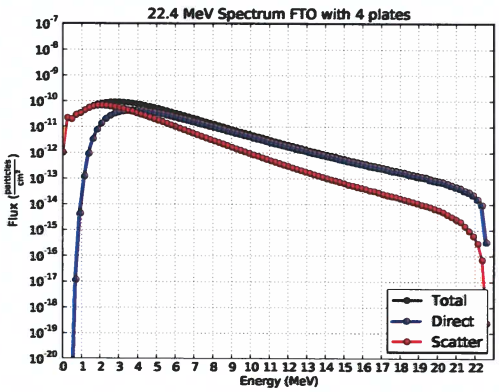

(b) 22.4 MeV FTO Spectrum

Figure 8: Direct, scatter, and total radiation spectra filtered by an FTO with 4 plates for two different endpoint energies.

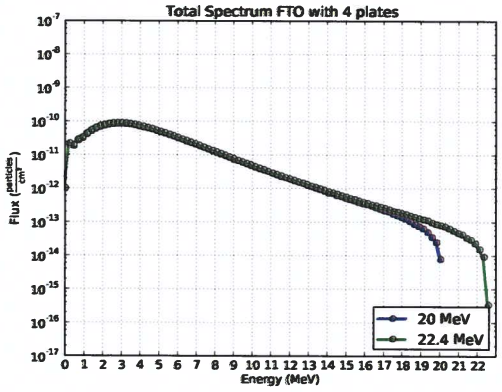

Figure 9: Total radiation spectra filtered by an FTO with 4 plates for two different endpoint energies.

4.2 Detector Responses for Cobalt 60 Source

We calculated the detector response for the different scintillator geometries and septa materials using a cobalt 60 source. In these calculations, we used a mono-energetic source of 1.25 MeV to compare our calculations to those performed by the University of Michigan. In reality, a cobalt 60 source contains two energies, 1.17 MeV and 1.33 MeV, and we expect this simplification to introduce some uncertainty between our calculated values and those measured experimentally.

The quantum efficiency, Swank factor, and DQE(0) values for the scintillator thicknesses and septa materials with a 1.095 mm pixel pitch are listed in Table 8 and for the 1.302 mm pixel pitch are listed in Table 9.

Overall, the quantum efficiency, Swank factor, and DQE(0) are larger for the larger pixel pitches. Stainless steel septa material produces larger quantum efficiency, Swank factor, and DQE(0). In all cases, the three detector parameters increase with increasing scintillator

Table 8: Geometry: 1.095 mm pixel pitch. The quantum efficiency, swank factor, and DQE(0) for different scintillator thickness and septa material using a cobalt 60 source.

Crystal	LSO	LSO	LSO	LSO	LSO	LSO
Pitch (mm)	1.095	1.095	1.095	1.095	1.095	1.095
Thickness (mm)	40	45	50	40	45	50
Septa Material	SS	SS	SS	W	W	W
Quantum Efficiency	0.695	0.728	0.754	0.691	0.715	0.734
Swank Factor	0.770	0.780	0.789	0.699	0.705	0.710
DQE(0)	0.535	0.567	0.595	0.483	0.504	0.521

Table 9: Geometry: 1.302 mm pixel pitch. The quantum efficiency, swank factor, and DQE(0) for different scintillator thickness and septa material using a cobalt 60 source.

Crystal	LSO	LSO	LSO	LSO	LSO	LSO	LYSO
Pitch (mm)	1.302	1.302	1.302	1.302	1.302	1.302	1.302
Thickness (mm)	40	45	50	40	45	50	50
Septa Material	SS	SS	SS	W	W	W	W
Quantum Efficiency	0.709	0.741	0.768	0.710	0.736	0.756	0.747
Swank Factor	0.786	0.797	0.806	0.725	0.732	0.738	0.733
DQE(0)	0.557	0.591	0.619	0.515	0.539	0.558	0.547

thickness. These results are illustrated in Figure 10.

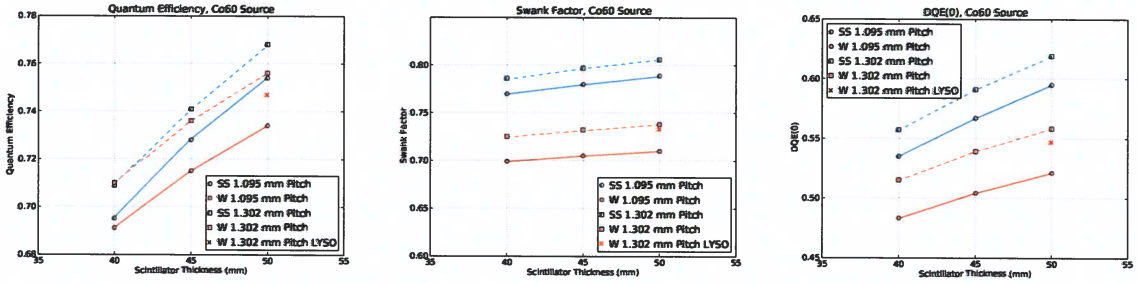

(a) Co60: Quantum Efficiency **(b)** Co60: Swank Factor **(c)** Co60: DQE(0)

Figure 10: Quantum efficiency, Swank factor, and DQE(0) using a cobalt 60 source for pixel pitches 1.095 mm and 1.302; thicknesses 40 mm, 45 mm, and 50 mm; and septa material stainless steel and tungsten alloy.

The percent differences in the detector responses due to different scintillator pitches are shown in Figure 11. The quantum efficiency is larger for for the larger pixel pitch by ≈2% for stainless steel septa and ≈3% for tungsten septa. The Swank factor is ≈2% larger for the larger pixel pitch and stainless steel septa, and ≈4% larger for the larger pixel pitch and tungsten septa. Overall, DQE(0) is larger for the larger pixel pitch, ≈4% for stainless steel septa and >6% for tungsten septa.

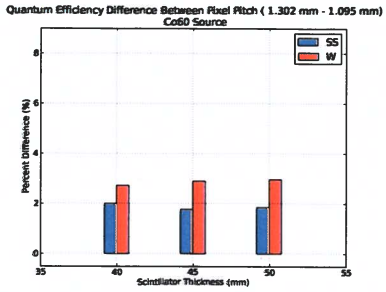

(a) Co60: Quantum Efficiency

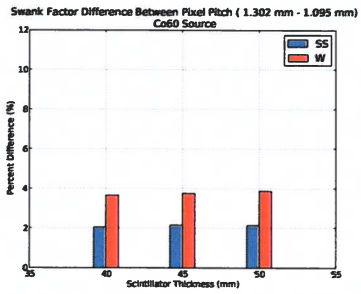

(b) Co60: Swank Factor

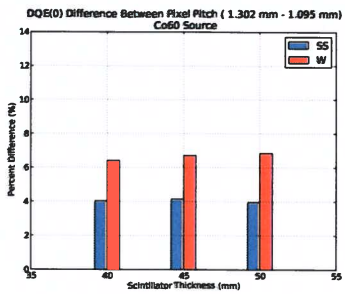

(c) Co60: DQE(0)

Figure 11: The percent differences in quantum efficiency, Swank factor, and DQE(0) using a cobalt 60 source due to pixel pitches (1.302 mm - 1.095); for thicknesses 40 mm, 45 mm, and 50 mm; and septa material stainless steel and tungsten alloy.

The percent differences in the detector responses due to the different septa materials are shown in Figure 12. The quantum efficiency is larger for the stainless steel septa compared to the tungsten septa, except for the the case of 1.032 pixel pitch and 40 mm thick. For both pixel pitches, the quantum efficiency percent difference grows with increasing thickness. The Swank factor is ≈10% larger for the stainless steel septa than tungsten alloy septa, for 1.095 mm pixel pitch and ≈8% larger for the 1.302 pixel pitch. These percentages are slightly larger with increasing scintillator thickness. The DQE(0) are larger for the stainless steel septa material with values ranging from 10–13% for increasing scintillator thickness for the 1.095 mm pixel pitch. Slightly lower values for the 1.302 mm pixel pitch range from 8-10%, increasing with scintillator thickness.

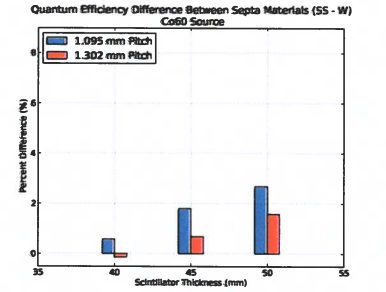

(a) Co60: Quantum Efficiency

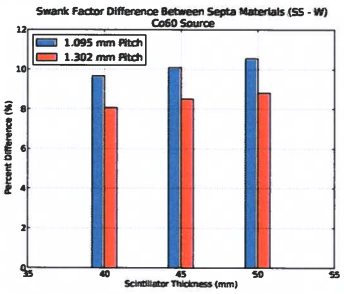

(b) Co60: Swank Factor

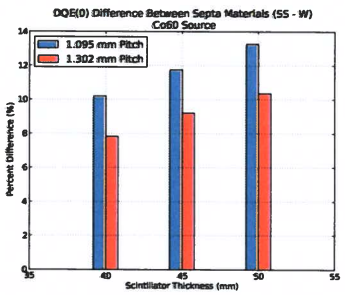

(c) Co60: DQE(0)

Figure 12: The percent differences in quantum efficiency, Swank factor, and DQE(0) using a cobalt 60 source due to septa material (stainless steel - tungsten alloy); for thicknesses 40 mm, 45 mm, and 50 mm; and pixel pitches 1.302 mm and 1.095.

Comparing the scintillator materials, LSO and LYSO, using a 1.302 mm pixel pitch, 50 mm scintillator thickness, and tungsten septa material yielded larger values for the quantum efficiency in LSO by ≈1% (Figure 13). The Swank factor was slightly larger for LSO (0.7%) and overall the DQE(0) value was larger for LSO (2%) compared to LYSO.

A comparison of the quantum efficiency, Swank factor, and DQE(0) to different scintillator thicknesses is shown in Figure 14. The quantum efficiency is larger for thicker scintillator

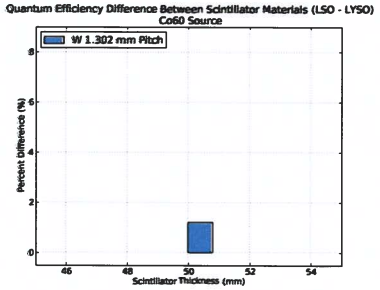

(a) Co60: Quantum Efficiency

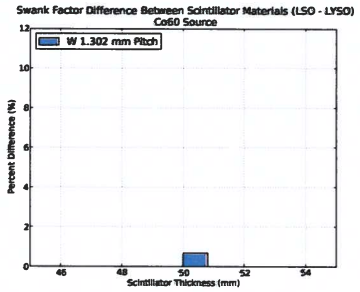

(b) Co60: Swank Factor

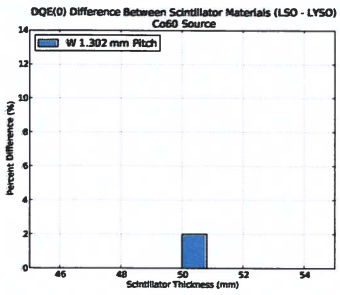

(c) Co60: DQE(0)

Figure 13: The percent differences in quantum efficiency, Swank factor, and DQE(0) using a cobalt 60 source due to different scintillator materials (LSO - LYSO), for tungsten alloy septa material, 1.302 mm pixel pitches, and 50 mm thicknesses.

designs. For stainless steel septa material, the quantum efficiency is >4% larger for a thickness of 45 mm compared to 40 mm for both pixel pitches, and ≈8% for a thickness of 50 mm compared to 40 mm. For tungsten alloy septa material, the quantum efficiency is >3% larger for a thickness of 45 mm compared to 40 mm for both pixel pitches, and ≈6% for a thickness of 50 mm compared to 40 mm. The Swank factor is larger for increasing scintillator thickness with the percent difference being larger for the stainless steel septa material than tungsten alloy. Overall, DQE(0) is larger with increasing scintillator thickness, showing the same trend of larger percent differences for stainless steel septa than tungsten alloy. For both pixel pitches using stainless steel septa, DQE(0) increases ≈6% and >10% for the 45 mm and 50 mm thicknesses, respectively. Similarly, for both pixel pitches using tungsten alloy septa, DQE(0) increases ≈4% and ≈8% for the 45 mm and 50 mm thicknesses, respectively.

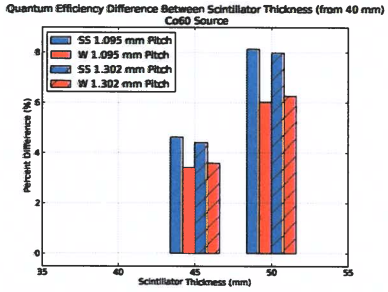

(a) Co60: Quantum Efficiency

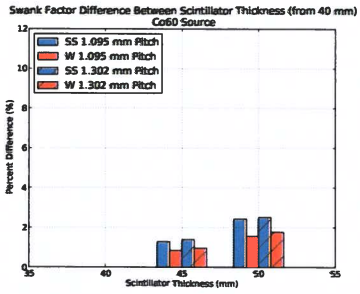

(b) Co60: Swank Factor

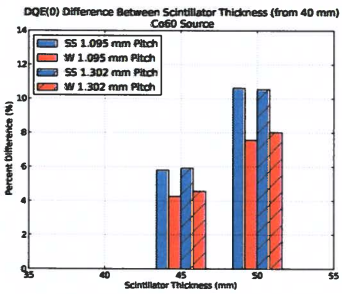

(c) Co60: DQE(0)

Figure 14: The percent differences in quantum efficiency, Swank factor, and DQE(0) using a cobalt 60 source due to scintillator thicknesses (difference from 40 mm); for septa material stainless steel and tungsten alloy; and pixel pitches 1.302 mm and 1.095.

4.3 Detector Responses for 20 MeV Spectrum Filtered by a Flat Field

We calculated the detector response for the different scintillator geometries and septa materials using a 20 MeV bremsstrahlung spectrum filtered by a flat field using 7 cm tungsten. Since this is the spectrum at DARHT Axis 1, these results may be compared to experimental data.

The quantum efficiency, Swank factor, and DQE(0) values for the scintillator thicknesses and septa materials with a 1.095 mm and 1.302 pixel pitches are listed in Table 10 and Table 11, respectively.

Table 10: Geometry: 1.095 mm pixel pitch. The swank factor, quantum efficiency, and DQE(0) for different scintillator thickness and septa material using a 20 MeV source filtered by a flat field.

Crystal	LSO	LSO	LSO	LSO	LSO	LSO
Pitch (mm)	1.095	1.095	1.095	1.095	1.095	1.095
Thickness (mm)	40	45	50	40	45	50
Septa Material	SS	SS	SS	W	W	W
Quantum Efficiency	0.632	0.668	0.699	0.702	0.730	0.754
Swank Factor	0.596	0.603	0.609	0.594	0.599	0.603
DQE(0)	0.377	0.402	0.425	0.417	0.437	0.454

Table 11: Geometry: 1.302 mm pixel pitch. The swank factor, quantum efficiency, and DQE(0) for different scintillator thickness and septa material using a 20 MeV source filtered by a flat field.

Crystal	LSO	LSO	LSO	LSO	LSO	LSO
Pitch (mm)	1.302	1.302	1.302	1.302	1.302	1.302
Thickness (mm)	40	45	50	40	45	50
Septa Material	SS	SS	SS	W	W	W
Quantum Efficiency	0.643	0.679	0.710	0.704	0.733	0.758
Swank Factor	0.599	0.606	0.612	0.598	0.603	0.607
DQE(0)	0.385	0.411	0.435	0.421	0.442	0.460

A comparison of the detector responses for the different scintillator designs is shown in Figure 15. Overall, the quantum efficiency, Swank factor, and DQE(0) are larger for the larger pixel pitches. Opposite than the cobalt 60 data, tungsten alloy septa material produces larger quantum efficiency and DQE(0). In all cases, the three detector parameters increase with increasing scintillator thickness.

The percent differences in the detector responses due to different scintillator pitches are shown in Figure 16. The quantum efficiency is larger for for the larger pixel pitch by <2% for stainless steel septa and <1% for tungsten septa. The Swank factor is <1% larger for the larger pixel pitch for both the stainless steel and tungsten alloy septa, with slightly larger

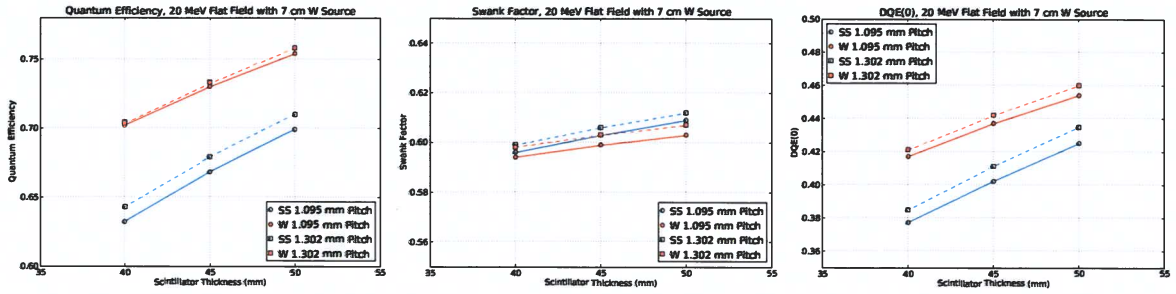

(a) 20MeV Flat Field: Quantum Efficiency

(b) 20MeV Flat Field: Swank Factor

(c) 20MeV Flat Field: DQE(0)

Figure 15: Quantum efficiency, Swank factor, and DQE(0) using a 20 MeV bremsstrahlung source filtered by a flat field with 7 cm tungsten for pixel pitches 1.095 mm and 1.302; thicknesses 40 mm, 45 mm, and 50 mm; and septa material stainless steel and tungsten alloy.

increases for the tungsten alloy septa. Overall, DQE(0) is larger for the larger pixel pitch, ≈2% for stainless steel septa and >1% for tungsten septa.

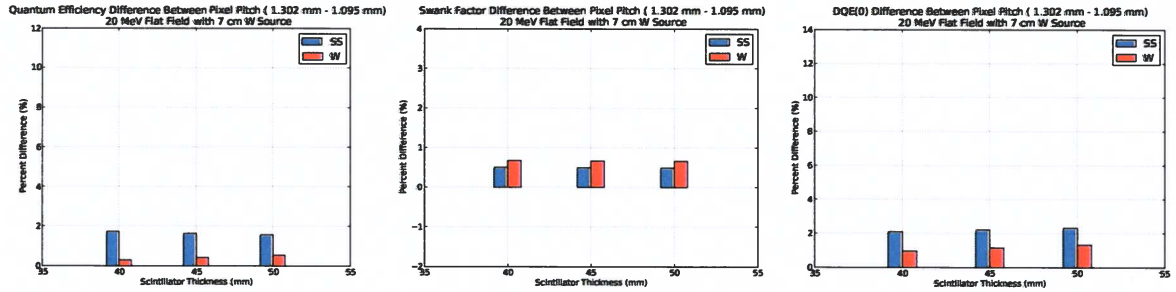

(a) 20MeV Flat Field: Quantum Efficiency

(b) 20MeV Flat Field: Swank Factor

(c) 20MeV Flat Field: DQE(0)

Figure 16: The percent differences in quantum efficiency, Swank factor, and DQE(0) using a 20 MeV bremsstrahlung source filtered by a flat field with 7 cm tungsten due to pixel pitches (1.302 mm - 1.095); for thicknesses 40 mm, 45 mm, and 50 mm; and septa material stainless steel and tungsten alloy.

The percent differences in the detector responses due to the different septa materials are shown in Figure 17. Note that the difference is (tungsten alloy - stainless steel), which is opposite of the plots for the cobalt 60 data. The quantum efficiency is larger for the tungsten alloy septa compared to the stainless steel (≈6–10%). For both pixel pitches, the quantum efficiency percent difference decreases with increasing thickness. The Swank factor is smaller for tungsten alloy than stainless steel septa, and the difference increases with scintillator thickness. Overall, DQE(0) is larger for the tungsten alloy septa material with values ranging from 6–10%. The DQE(0) differences decrease with increasing scintillator thickness. The percent difference is larger for the 1.095 pixel pitch than the 1.302 pixel pitch.

A comparison of the quantum efficiency, Swank factor, and DQE(0) to different scintillator thicknesses is shown in Figure 18. The quantum efficiency is larger for thicker scintillator

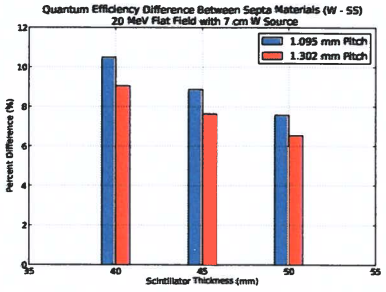

(a) 20MeV Flat Field: Quantum Efficiency

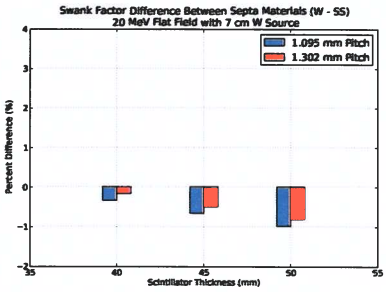

(b) 20MeV Flat Field: Swank Factor

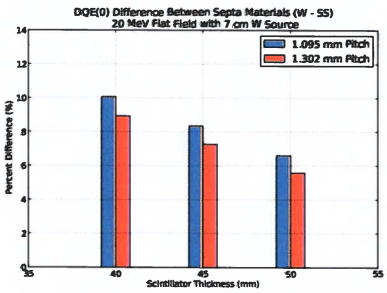

(c) 20MeV Flat Field: DQE(0)

Figure 17: The percent differences in quantum efficiency, Swank factor, and DQE(0) using a 20 MeV bremsstrahlung source filtered by a flat field with 7 cm tungsten due to septa material (tungsten alloy - stainless steel); for pixel pitches 1.302 mm and 1.095; and thicknesses 40 mm, 45 mm, and 50 mm.

designs. For stainless steel septa material, the quantum efficiency is >5% larger for a thickness of 45 mm compared to 40 mm for both pixel pitches, and ≈10% for a thickness of 50 mm compared to 40 mm. For tungsten alloy septa material, the quantum efficiency is ≈4% larger for a thickness of 45 mm compared to 40 mm for both pixel pitches, and >7% for a thickness of 50 mm compared to 40 mm. The Swank factor is larger for increasing scintillator thickness with the percent difference being larger for the stainless steel septa material than tungsten alloy. Overall, DQE(0) is larger with increasing scintillator thickness, showing the same trend of larger percent differences for stainless steel septa than tungsten alloy. For both pixel pitches using stainless steel septa, DQE(0) increases >6% and ≈12% for the 45 mm and 50 mm thicknesses, respectively. Similarly, for both pixel pitches using tungsten alloy septa, DQE(0) increases ≈5% and >8% for the 45 mm and 50 mm thicknesses, respectively.

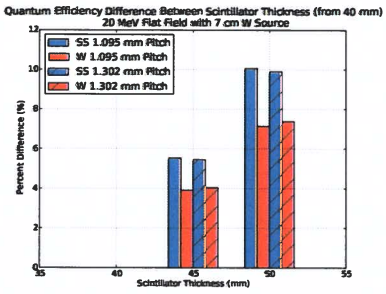

(a) 20MeV Flat Field: Quantum Efficiency

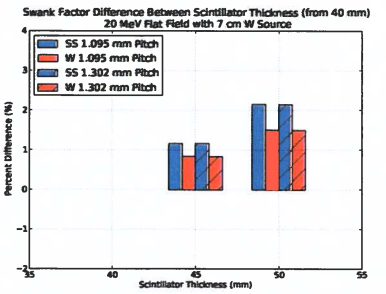

(b) 20MeV Flat Field: Swank Factor

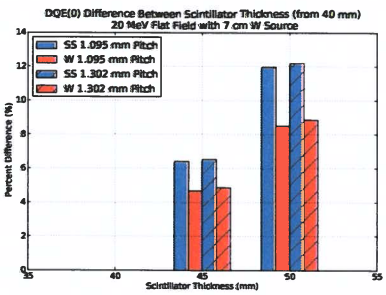

(c) 20MeV Flat Field: DQE(0)

Figure 18: The percent differences in quantum efficiency, Swank factor, and DQE(0) using a 20 MeV bremsstrahlung source filtered by a flat field with 7 cm tungsten due to scintillator thicknesses (difference from 40 mm); for septa material stainless steel and tungsten alloy; and pixel pitches 1.302 mm and 1.095.

4.4 Detector Responses for 22.4 MeV Spectrum Filtered by a Flat Field

We calculated the detector response for the different scintillator geometries and septa materials using a 22.4 MeV bremsstrahlung spectrum filtered by a flat field using 7 cm tungsten. This is the anticipated spectrum to be used at ECSE.

The quantum efficiency Swank factor, and DQE(0) values for the scintillator thicknesses and septa materials with a 1.095 mm and 1.302 pixel pitches are listed in Table 12 and Table 13, respectively.

Table 12: Geometry: 1.095 mm pixel pitch. The swank factor, quantum efficiency, and DQE(0) for different scintillator thickness and septa material using a 22.4 MeV bremsstrahlung source filtered by a flat field.

Crystal	LSO	LSO	LSO	LSO	LSO	LSO
Pitch (mm)	1.095	1.095	1.095	1.095	1.095	1.095
Thickness (mm)	40	45	50	40	45	50
Septa Material	SS	SS	SS	W	W	W
Quantum Efficiency	0.633	0.669	0.699	0.702	0.730	0.754
Swank Factor	0.582	0.589	0.595	0.582	0.587	0.590
DQE(0)	0.369	0.394	0.416	0.409	0.428	0.445

Table 13: Geometry: 1.302 mm pixel pitch. The swank factor, quantum efficiency, and DQE(0) for different scintillator thickness and septa material using a 22.4 MeV bremsstrahlung source filtered by a flat field.

Crystal	LSO	LSO	LSO	LSO	LSO	LSO
Pitch (mm)	1.302	1.302	1.302	1.302	1.302	1.302
Thickness (mm)	40	45	50	40	45	50
Septa Material	SS	SS	SS	W	W	W
Quantum Efficiency	0.644	0.680	0.711	0.704	0.733	0.758
Swank Factor	0.586	0.592	0.598	0.585	0.590	0.595
DQE(0)	0.377	0.403	0.425	0.412	0.433	0.451

A comparison of the detector responses for the different scintillator designs is shown in Figure 19. Overall, the quantum efficiency, Swank factor, and DQE(0) are larger for the larger pixel pitches. Opposite than the cobalt 60 data, tungsten alloy septa material produces larger quantum efficiency and DQE(0). In all cases, the three detector parameters increase with increasing scintillator thickness.

The percent differences in the detector responses due to different scintillator pitches are shown in Figure 20. The quantum efficiency is larger for the larger pixel pitch by $\approx$2% for stainless steel septa and <1% for tungsten septa. The Swank factor is <1% larger for the

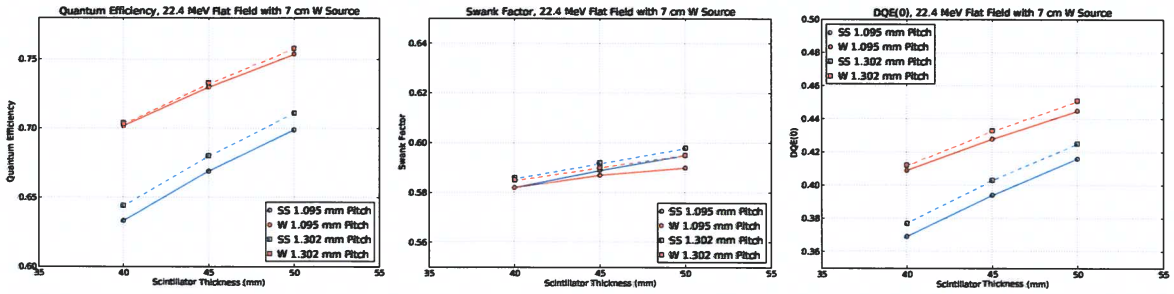

(a) 22.4 MeV Flat Field: Quantum Efficiency **(b)** 22.4 MeV Flat Field: Swank Factor **(c)** 22.4 MeV Flat Field: DQE(0)

Figure 19: Quantum efficiency, Swank factor, and DQE(0) using a 22.4 MeV bremsstrahlung source filtered by a flat field for pixel pitches 1.095 mm and 1.302; thicknesses 40 mm, 45 mm, and 50 mm; and septa material stainless steel and tungsten alloy.

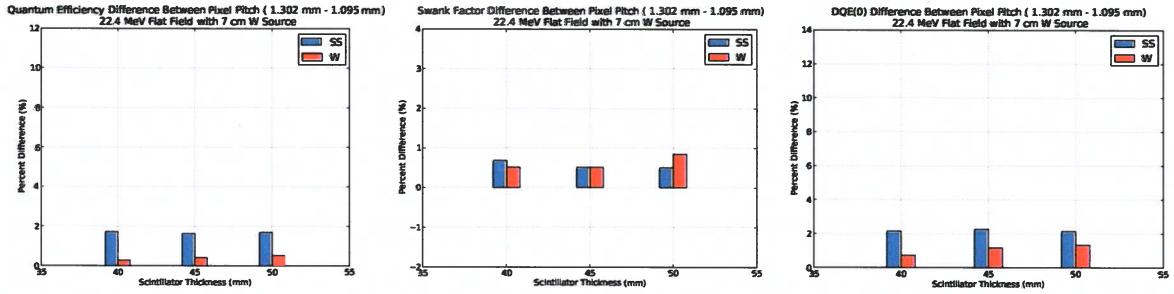

(a) 22.4 MeV Flat Field: Quantum Efficiency **(b)** 22.4 MeV Flat Field: Swank Factor **(c)** 22.4 MeV Flat Field: DQE(0)

Figure 20: The percent differences in quantum efficiency, Swank factor, and DQE(0) using a 22.4 MeV bremsstrahlung source filtered by a flat field for pixel pitches 1.302 mm and 1.095; thicknesses 40 mm, 45 mm, and 50 mm; and septa material stainless steel and tungsten alloy.

larger pixel pitch for both the stainless steel and tungsten alloy septa. Overall, DQE(0) is larger for the larger pixel pitch, ≈2% for stainless steel septa and ≈1% for tungsten septa.

The percent differences in the detector responses due to the different septa materials are shown in Figure 21. Note that the difference is (tungsten alloy - stainless steel), which is opposite of the plots for the cobalt 60 data. The quantum efficiency is larger for the tungsten alloy septa compared to the stainless steel (≈6–10%). For both pixel pitches, the quantum efficiency percent difference decreases with increasing thickness. The Swank factor is smaller for tungsten alloy than stainless steel septa, and the difference increases with scintillator thickness. Overall, DQE(0) is larger for the tungsten alloy septa material with values ranging from 6–10%. The DQE(0) differences decrease with increasing scintillator thickness. The percent difference is larger for the 1.095 pixel pitch than the 1.302 pixel pitch.

A comparison of the quantum efficiency, Swank factor, and DQE(0) to different scintillator thicknesses is shown in Figure 22. The quantum efficiency is larger for thicker scintillator designs. For stainless steel septa material, the quantum efficiency is >5% larger for a thick-

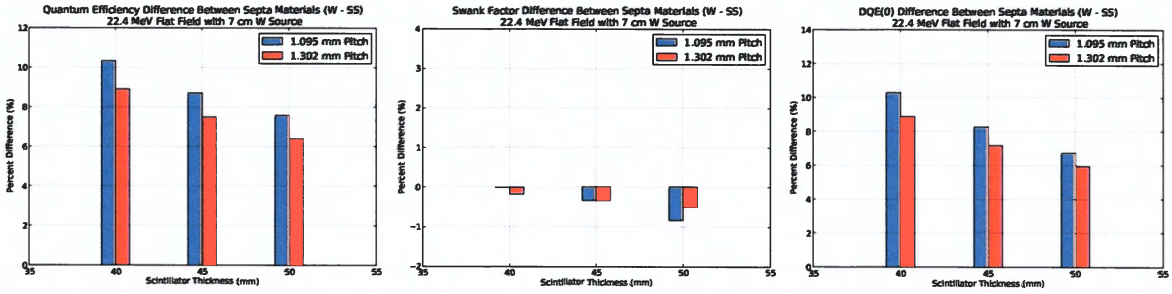

(a) 22.4 MeV Flat Field: Quantum Efficiency **(b)** 22.4 MeV Flat Field: Swank Factor **(c)** 22.4 MeV Flat Field: DQE(0)

Figure 21: The percent differences in quantum efficiency, Swank factor, and DQE(0) using a 22.4 MeV bremsstrahlung source filtered by a flat field for septa material stainless steel and tungsten alloy; pixel pitches 1.302 mm and 1.095; and thicknesses 40 mm, 45 mm, and 50 mm.

ness of 45 mm compared to 40 mm for both pixel pitches, and ≈10% for a thickness of 50 mm compared to 40 mm. For tungsten alloy septa material, the quantum efficiency is ≈4% larger for a thickness of 45 mm compared to 40 mm for both pixel pitches, and >7% for a thickness of 50 mm compared to 40 mm. The Swank factor is larger for increasing scintillator thickness with the percent difference being larger for the stainless steel septa material than tungsten alloy. Overall, DQE(0) is larger with increasing scintillator thickness, showing the same trend of larger percent differences for stainless steel septa than tungsten alloy. For both pixel pitches using stainless steel septa, DQE(0) increases >6% and ≈12% for the 45 mm and 50 mm thicknesses, respectively. Similarly, for both pixel pitches using tungsten alloy septa, DQE(0) increases ≈5% and >8% for the 45 mm and 50 mm thicknesses, respectively.

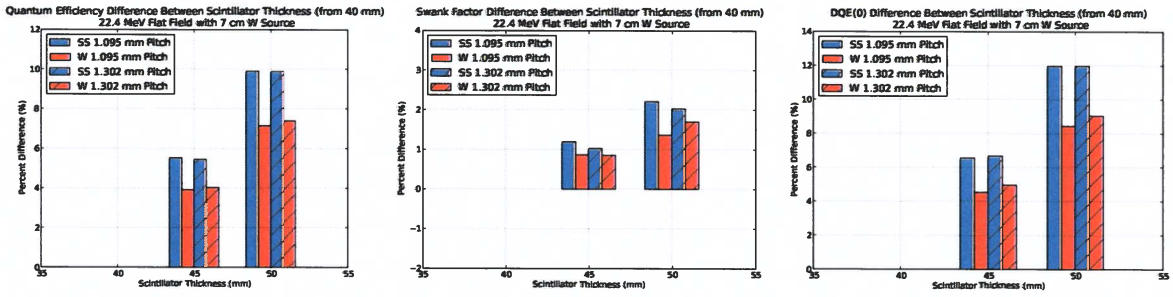

(a) 22.4 MeV Flat Field: Quantum Efficiency **(b)** 22.4 MeV Flat Field: Swank Factor **(c)** 22.4 MeV Flat Field: DQE(0)

Figure 22: The percent differences in quantum efficiency, Swank factor, and DQE(0) using a 22.4 MeV bremsstrahlung source filtered by a flat field for scintillator thicknesses 40 mm, 45 mm, and 50 mm; septa material stainless steel and tungsten alloy; and pixel pitches 1.302 mm and 1.095.

4.5 Detector Responses for 20 MeV Spectrum Filtered by an FTO

We calculated the detector response for the different scintillator geometries and septa materials using a 20 MeV bremsstrahlung spectrum filtered by an FTO with four plates.

The quantum efficiency Swank factor, and DQE(0) values for the scintillator thicknesses and septa materials with a 1.095 mm and 1.302 pixel pitches are listed in Table 14 and Table 15, respectively.

Table 14: Geometry: 1.095 mm pixel pitch. The swank factor, quantum efficiency, and DQE(0) for different scintillator thickness and septa material using a 20 MeV bremsstrahlung source filtered by an FTO with four plates.

Crystal	LSO	LSO	LSO	LSO	LSO	LSO
Pitch (mm)	1.095	1.095	1.095	1.095	1.095	1.095
Thickness (mm)	40	45	50	40	45	50
Septa Material	SS	SS	SS	W	W	W
Quantum Efficiency	0.635	0.670	0.700	0.696	0.723	0.747
Swank Factor	0.610	0.617	0.624	0.604	0.609	0.614
DQE(0)	0.387	0.414	0.437	0.420	0.440	0.458

Table 15: Geometry: 1.302 mm pixel pitch. The swank factor, quantum efficiency, and DQE(0) for different scintillator thickness and septa material using a 20 MeV bremsstrahlung source filtered by an FTO with four plates.

Crystal	LSO	LSO	LSO	LSO	LSO	LSO
Pitch (mm)	1.302	1.302	1.302	1.302	1.302	1.302
Thickness (mm)	40	45	50	40	45	50
Septa Material	SS	SS	SS	W	W	W
Quantum Efficiency	0.646	0.681	0.712	0.699	0.728	0.753
Swank Factor	0.613	0.621	0.628	0.608	0.614	0.619
DQE(0)	0.396	0.423	0.447	0.425	0.447	0.466

A comparison of the detector responses for the different scintillator designs is shown in Figure 23. Overall, the quantum efficiency, Swank factor, and DQE(0) are larger for the larger pixel pitches. Opposite than the cobalt 60 data, tungsten alloy septa material produces larger quantum efficiency and DQE(0). In all cases, the three detector parameters increase with increasing scintillator thickness.

The percent differences in the detector responses due to different scintillator pitches are shown in Figure 24. The quantum efficiency is larger for the larger pixel pitch by <2% for stainless steel septa and <1% for tungsten septa. The Swank factor is <1% larger for the larger pixel pitch for both the stainless steel and tungsten alloy septa. Overall, DQE(0) is larger for the larger pixel pitch, >2% for stainless steel septa and <1% for tungsten septa.

The percent differences in the detector responses due to the different septa materials are shown in Figure 25. Note that the difference is (tungsten alloy - stainless steel), which is opposite of the plots for the cobalt 60 data. The quantum efficiency is larger for the tungsten alloy septa compared to the stainless steel (≈6–9%). For both pixel pitches, the quantum efficiency percent difference decreases with increasing thickness. The Swank factor

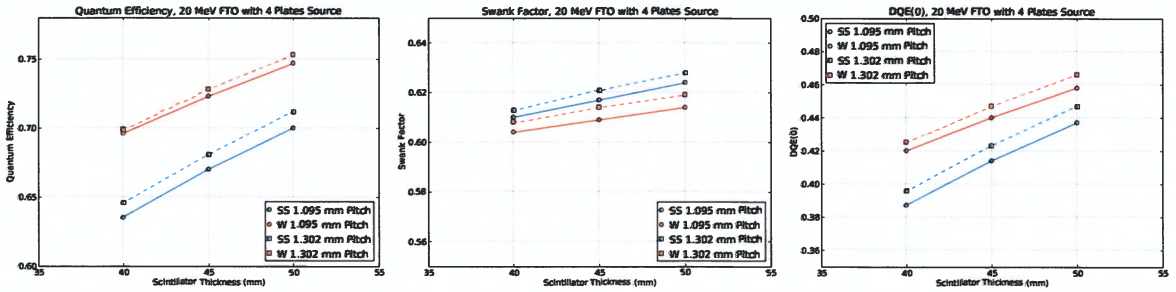

(a) 20 MeV FTO: Quantum Efficiency

(b) 20 MeV FTO: Swank Factor

(c) 20 MeV FTO: DQE(0)

Figure 23: Quantum efficiency, Swank factor, and DQE(0) using a 20 MeV bremsstrahlung source filtered by an FTO with four plates for pixel pitches 1.095 mm and 1.302; thicknesses 40 mm, 45 mm, and 50 mm; and septa material stainless steel and tungsten alloy.

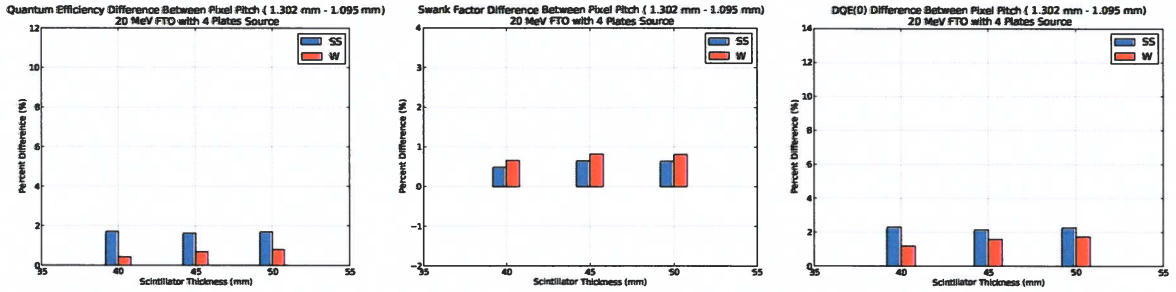

(a) 20 MeV FTO: Quantum Efficiency

(b) 20 MeV FTO: Swank Factor

(c) 20 MeV FTO: DQE(0)

Figure 24: The percent differences in quantum efficiency, Swank factor, and DQE(0) using a 20 MeV bremsstrahlung source filtered by an FTO with four plates for pixel pitches 1.302 mm and 1.095; thicknesses 40 mm, 45 mm, and 50 mm; and septa material stainless steel and tungsten alloy.

is smaller for tungsten alloy than stainless steel septa, and the difference increases with scintillator thickness. Overall, DQE(0) is larger for the tungsten alloy septa material with values ranging from 4–8%. The DQE(0) differences decrease with increasing scintillator thickness. The percent differences are larger for the 1.095 pixel pitch than the 1.302 pixel pitch.

A comparison of the quantum efficiency, Swank factor, and DQE(0) to different scintillator thicknesses is shown in Figure 26. The quantum efficiency is larger for thicker scintillator designs. For stainless steel septa material, the quantum efficiency is >5% larger for a thickness of 45 mm compared to 40 mm for both pixel pitches, and <10% for a thickness of 50 mm compared to 40 mm. For tungsten alloy septa material, the quantum efficiency is ≈4% larger for a thickness of 45 mm compared to 40 mm for both pixel pitches, and >7% for a thickness of 50 mm compared to 40 mm. The Swank factor is larger for increasing scintillator thickness with the percent difference being larger for the stainless steel septa material than tungsten alloy. Overall, DQE(0) is larger with increasing scintillator thickness, showing the same trend of larger percent differences for stainless steel septa than tungsten alloy. For both

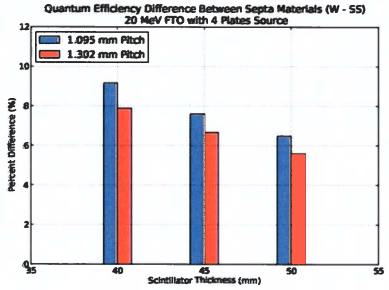

(a) 20 MeV FTO: Quantum Efficiency

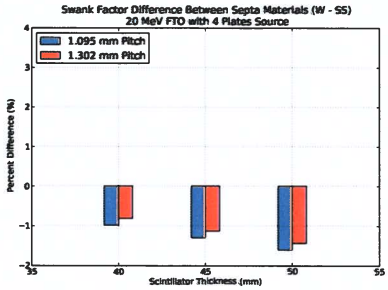

(b) 20 MeV FTO: Swank Factor

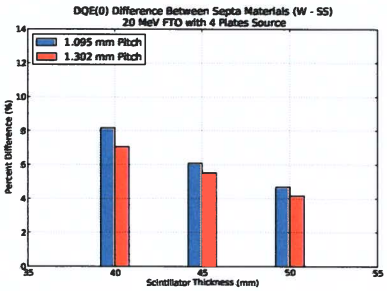

(c) 20 MeV FTO: DQE(0)

Figure 25: The percent differences in quantum efficiency, Swank factor, and DQE(0) using a 20 MeV bremsstrahlung source filtered by an FTO with four plates for septa material stainless steel and tungsten alloy; pixel pitches 1.302 mm and 1.095; and thicknesses 40 mm, 45 mm, and 50 mm.

pixel pitches using stainless steel septa, DQE(0) increases >6% and ≈12% for the 45 mm and 50 mm thicknesses, respectively. Similarly, for both pixel pitches using tungsten alloy septa, DQE(0) increases ≈5% and ≈9% for the 45 mm and 50 mm thicknesses, respectively.

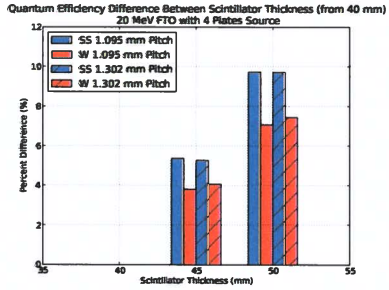

(a) 20 MeV FTO: Quantum Efficiency

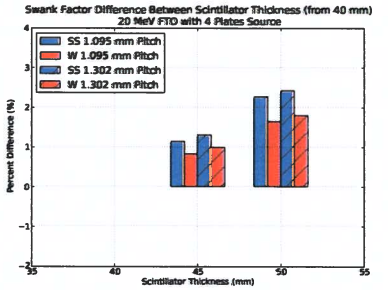

(b) 20 MeV FTO: Swank Factor

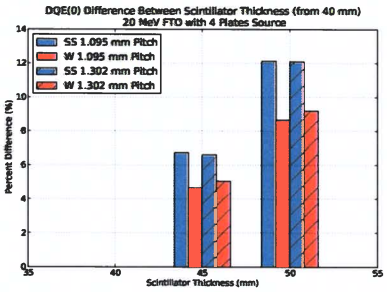

(c) 20 MeV FTO: DQE(0)

Figure 26: The percent differences in quantum efficiency, Swank factor, and DQE(0) using a 20 MeV bremsstrahlung source filtered by an FTO with four plates for scintillator thicknesses 40 mm, 45 mm, and 50 mm; septa material stainless steel and tungsten alloy; and pixel pitches 1.302 mm and 1.095.

4.6 Detector Responses for 22.4 MeV Spectrum Filtered by an FTO

We calculated the detector response for the different scintillator geometries and septa materials using a 22.4 MeV bremsstrahlung spectrum filtered by an FTO with four plates. This is the anticipated endpoint energy for ECSE.

The quantum efficiency Swank factor, and DQE(0) values for the scintillator thicknesses and septa materials with a 1.095 mm and 1.302 pixel pitches are listed in Table 16 and Table 17, respectively.

Table 16: Geometry: 1.095 mm pixel pitch. The swank factor, quantum efficiency, and DQE(0) for different scintillator thickness and septa material using a 22.4 MeV bremsstrahlung source filtered by an FTO with four plates.

Crystal	LSO	LSO	LSO	LSO	LSO	LSO
Pitch (mm)	1.095	1.095	1.095	1.095	1.095	1.095
Thickness (mm)	40	45	50	40	45	50
Septa Material	SS	SS	SS	W	W	W
Quantum Efficiency	0.636	0.670	0.701	0.696	0.723	0.746
Swank Factor	0.606	0.613	0.620	0.600	0.605	0.610
DQE(0)	0.385	0.411	0.435	0.417	0.438	0.455

Table 17: Geometry: 1.302 mm pixel pitch. The swank factor, quantum efficiency, and DQE(0) for different scintillator thickness and septa material using a 22.4 MeV bremsstrahlung source filtered by an FTO with four plates.

Crystal	LSO	LSO	LSO	LSO	LSO	LSO
Pitch (mm)	1.302	1.302	1.302	1.302	1.302	1.302
Thickness (mm)	40	45	50	40	45	50
Septa Material	SS	SS	SS	W	W	W
Quantum Efficiency	0.646	0.681	0.712	0.699	0.728	0.752
Swank Factor	0.609	0.617	0.624	0.604	0.610	0.615
DQE(0)	0.394	0.421	0.444	0.422	0.444	0.463

A comparison of the detector responses for the different scintillator designs is shown in Figure 27. Overall, the quantum efficiency, Swank factor, and DQE(0) are larger for the larger pixel pitches. Opposite than the cobalt 60 data, tungsten alloy septa material produces larger quantum efficiency and DQE(0). In all cases, the three detector parameters increase with increasing scintillator thickness.

The percent differences in the detector responses due to different scintillator pitches are shown in Figure 28. The quantum efficiency is larger for the larger pixel pitch by <2% for stainless steel septa and <1% for tungsten septa. The Swank factor is <1% larger for the larger pixel pitch for both the stainless steel and tungsten alloy septa. Overall, DQE(0) is larger for the larger pixel pitch, >2% for stainless steel septa and >1% for tungsten septa.

The percent differences in the detector responses due to the different septa materials are shown in Figure 29. Note that the difference is (tungsten alloy - stainless steel), which is opposite of the plots for the cobalt 60 data. The quantum efficiency is larger for the tungsten alloy septa compared to the stainless steel (≈6–9%). For both pixel pitches, the quantum efficiency percent differences decrease with increasing thickness. The Swank factor is smaller for tungsten alloy than stainless steel septa, and the differences increase with scintillator thickness. Overall, DQE(0) is larger for the tungsten alloy septa material with values ranging from ≈4–8%. The DQE(0) values decrease with increasing scintillator thickness. The percent differences are larger for the 1.095 pixel pitch than the 1.302 pixel pitch.

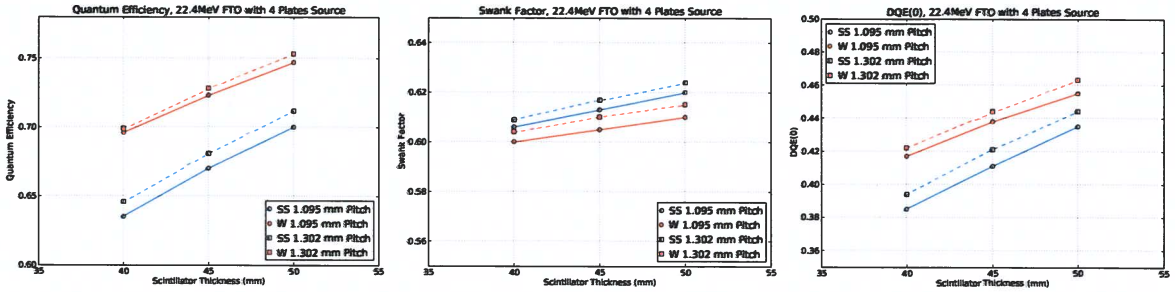

(a) 22.4 MeV FTO: Quantum Efficiency

(b) 22.4 MeV FTO: Swank Factor

(c) 22.4 MeV FTO: DQE(0)

Figure 27: Quantum efficiency, Swank factor, and DQE(0) using a 22.4 MeV bremsstrahlung source filtered by an FTO with four plates for pixel pitches 1.095 mm and 1.302; thicknesses 40 mm, 45 mm, and 50 mm; and septa material stainless steel and tungsten alloy.

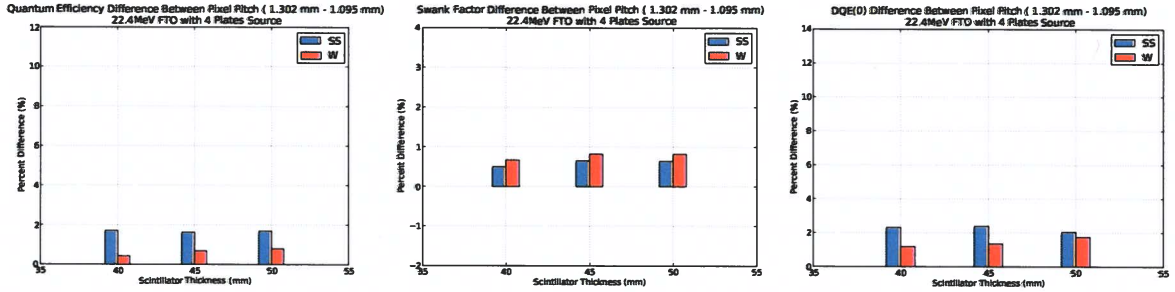

(a) 22.4 MeV FTO: Quantum Efficiency

(b) 22.4 MeV FTO: Swank Factor

(c) 22.4 MeV FTO: DQE(0)

Figure 28: The percent differences in quantum efficiency, Swank factor, and DQE(0) using a 22.4 MeV bremsstrahlung source filtered by an FTO with four plates for pixel pitches 1.302 mm and 1.095; thicknesses 40 mm, 45 mm, and 50 mm; and septa material stainless steel and tungsten alloy.

A comparison of the quantum efficiency, Swank factor, and DQE(0) to different scintillator thicknesses is shown in Figure 30. The quantum efficiency is larger for thicker scintillator designs. For stainless steel septa material, the quantum efficiency is >5% larger for a thickness of 45 mm compared to 40 mm for both pixel pitches, and <10% for a thickness of 50 mm compared to 40 mm. For tungsten alloy septa material, the quantum efficiency is ≈4% larger for a thickness of 45 mm compared to 40 mm for both pixel pitches, and >7% for a thickness of 50 mm compared to 40 mm. The Swank factor is larger for increasing scintillator thickness with the percent difference being larger for the stainless steel septa material than tungsten alloy. Overall, DQE(0) is larger with increasing scintillator thickness, showing the same trend of larger percent differences for stainless steel septa than tungsten alloy. For both pixel pitches using stainless steel septa, DQE(0) increases >6% and ≈12% for the 45 mm and 50 mm thicknesses, respectively. Similarly, for both pixel pitches using tungsten alloy septa, DQE(0) increases ≈5% and ≈9% for the 45 mm and 50 mm thicknesses, respectively.

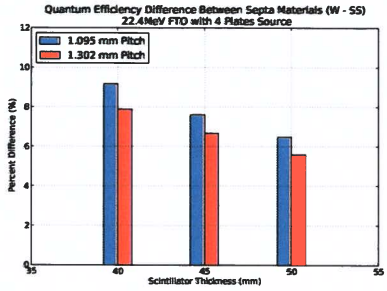

(a) 22.4 MeV FTO: Quantum Efficiency

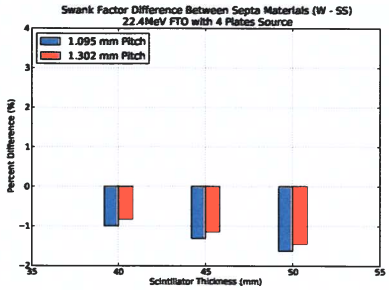

(b) 22.4 MeV FTO: Swank Factor

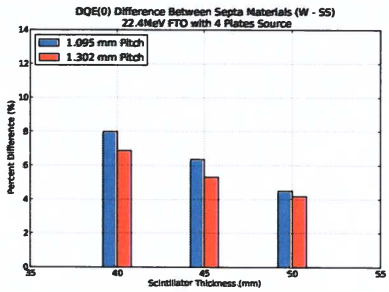

(c) 22.4 MeV FTO: DQE(0)

Figure 29: The percent differences in quantum efficiency, Swank factor, and DQE(0) using a 22.4 MeV bremsstrahlung source filtered by an FTO with four plates for septa material stainless steel and tungsten alloy; pixel pitches 1.302 mm and 1.095; and thicknesses 40 mm, 45 mm, and 50 mm.

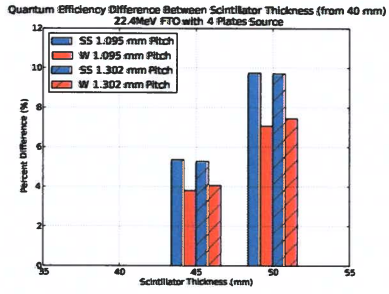

(a) 22.4 MeV FTO: Quantum Efficiency

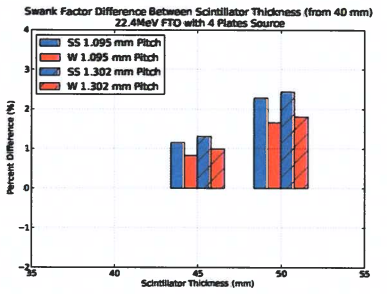

(b) 22.4 MeV FTO: Swank Factor

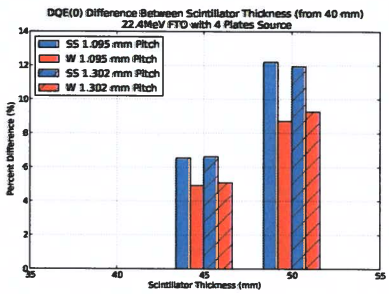

(c) 22.4 MeV FTO: DQE(0)

Figure 30: The percent differences in quantum efficiency, Swank factor, and DQE(0) using a 22.4 MeV bremsstrahlung source filtered by an FTO with four plates for scintillator thicknesses 40 mm, 45 mm, and 50 mm; septa material stainless steel and tungsten alloy; and pixel pitches 1.302 mm and 1.095.

5 Conclusions

Optimizing the scintillator design for high-energy x-ray radiography to be performed at ECSE can help provide the most robust data possible for the relatively limited amount of data that can be collected at this type of facility. We have calculated the detector response, which includes the quantum efficiency, Swank factor, and DQE(0), for thirteen different permutations of scintillator design. These permutations include two pixel pitches, 1.095 mm and 1.302 mm; two septa materials, stainless steel and tungsten alloy; and three scintillator thicknesses, 40 mm, 45 mm, and 50 mm. In addition, two different scintillating materials were investigated: LSO and LYSO. Five different input spectra were used to calculate the detector responses: cobalt 60, 20 MeV bremsstrahlung spectrum filtered by a flat field, 22.4 MeV bremsstrahlung spectrum filtered by a flat field, 20 MeV bremsstrahlung spectrum filtered by and FTO with four plates, and 22.4 MeV bremsstrahlung spectrum filtered by and FTO with four plates.

The detector responses using a cobalt 60 source showed larger DQE(0) for thicker scin-

tillator designs. The stainless steel septa had larger DQE(0) than tungsten alloy septa. The larger pixel pitch, 1.302 mm, had larger DQE(0) compared to the smaller pixel pitch, 1.095 mm. These results will be compared to experimental measurements of prototype scintillator designs to validate the calculations. These simulations irradiated the center region of the scintillator to allow for scatter within the scintillator and give theoretical detector responses. In reality, the entire scintillator will be irradiated. Furthermore, these calculations used a single x-ray energy of 1.25 MeV whereas a cobalt 60 source has a dual energy of 1.17 and 1.33 MeV. We compared our calculations to those from the University of Michigan where they used the code EGSnrc and EGS++ and found very good agreement. Due to the difference in the simulation setup and the experimental setup, we expect some uncertainty between our calculations and the experimental measurements.

Detector responses were calculated using 20 MeV and 22.4 MeV bremsstrahlung sources filtered by a flat field with 7 cm of tungsten in the bullnose. The 20 MeV endpoint energy spectrum is that of DARHT Axis 1 and these detector responses may be measured experimentally to validate these calculations. The 22.4 MeV spectrum is proposed for ECSE and gives an indication of the detector response for this facility. Overall, we found that DQE(0) increases with thicker scintillator designs, is larger for tungsten alloy septa, and is larger for the larger pixel pitch. The scintillator design effects on the Swank factor ranged from $\approx$1–2%. The largest effects on DQE(0) resulted from changes in the quantum efficiency. Pixel pitch had the smallest effect on DQE(0), $\approx$1–2%. Changing the septa material changed DQE(0) by $\approx$ 6–10% and changing the scintillator thickness changed DQE(0) by $\approx$5–12%. The largest increases in DQE(0) come from using tungsten alloy septa material and increasing the thickness to 50 mm.

Finally, the detector responses were calculated using 20 MeV and 22.4 MeV bremsstrahlung sources filtered by an FTO with four plates. The detector responses in this regime are of interest as they give an indication of detector performance for hydrotest data. The spectra filtered by an FTO has much more scatter than the spectra filtered by a flat field, due to scatter being produced by the object and impinging on the scintillator. As such, there is a larger contribution of low-energy x-rays from scattered radiation for the FTO spectra compared to the flat field spectra. The detector responses for the two spectra filtered by an FTO showed a similar trend to the flat field detector responses where DQE(0) was larger for thicker scintillator designs, tungsten alloy septa, and larger pixel pitch. The Swank factor varied around 1–2% for different scintillator designs. The largest impact came from the difference in quantum efficiency from the different designs. The largest trade offs for achieving the largest quantum efficiency and DQE(0) were to use tungsten alloy septa material and a scintillator thickness of 50 mm. The differences in DQE(0) due to pixel pitch were around 1–2%, whereas using tungsten alloy septa material increased DQE(0) 4–8%, and increasing the thickness increased DQE(0) by 8–12%.

In all four of the detector responses using poly-energetic sources, the largest DQE(0) resulted from the scintillator design using 1.302 mm pixel pitch, tungsten alloy septa material, and 50 mm thick scintillator. A general ranking of the DQE(0) values is shown in Table 18. These rankings generalize the best scintillator designs for a poly-energetic spectra. If, for manufacturing limitations, the recommended design cannot be produced at the scale necessary, then the following recommendations are listed in order as alternatives for a scintillator design intended for ECSE.

Table 18: Rankings of the scintillator designs that produce the largest DQE(0) for the poly-energetic spectra.

Rank	Pitch (mm)	Septa Material	Thickness (mm)
1	1.302	W	50
2	1.095	W	50
3	1.302	W	45
4	1.302	SS	50

These results only take into account the zero-frequency DQE. The frequency-dependent DQE and optical photon effects should be taken into account prior to finalizing the scintillator design for ECSE in order to fully assess scintillator performance.

References

[1] R. Smith, *Assembly, LSO Crystal Testing*, 2019. Drawing Number H-340802-01.

[2] C. J. Werner, J. C. Armstrong, F. B. Brown, J. S. Bull, L. Casswell, L. J. Cox, D. A. Dixon, R. A. F. Iii, J. T. Goorley, H. G. I. Hughes, J. A. Favorite, R. L. Martz, S. G. Mashnik, M. E. Rising, C. J. J. Solomon, A. Sood, J. E. Sweezy, A. J. Zukaitis, C. A. Anderson, J. S. Elson, J. W. J. Durkee, R. C. Johns, G. W. Mckinney, G. E. McMath, J. S. Hendricks, D. B. Pelowitz, R. E. Prael, T. E. Booth, M. R. James, M. L. Fensin, T. Wilcox, and B. C. Kiedrowski, "Mcnp user's manual code version 6.2," tech. rep., 2017. Sponsor: U.S. Department of Homeland Security, DOE Nuclear Criticality Safety.

[3] R. K. Swank, "Absorption and noise in x-ray phosphors," *Journal of Applied Physics*, vol. 44, no. 9, pp. 4199–4203, 1973.

[4] J. L. Schei, M. R. James, and M. L. Klasky, "(U) endpoint energy and scintillator geometry effects on the swank factor, quantum efficiency, and DQE(0) for high-energy radiography," tech. rep., Los Alamos National Laboratory, 2020. LA-UR-20-27082.